



HAL
open science

Complex photonic response reveals 3D self-organization of structural colored bacterial colonies

Lukas Schertel, Gea van de Kerkhof, Gianni Jacucci, Laura Catón, Yu Ogawa, Bodo D. Wilts, Colin J Ingham, Silvia Vignolini, Villads Egede Johansen

► To cite this version:

Lukas Schertel, Gea van de Kerkhof, Gianni Jacucci, Laura Catón, Yu Ogawa, et al.. Complex photonic response reveals 3D self-organization of structural colored bacterial colonies. *rsif.royalsocietypublishing.org Research*, 2020, 10.1098/rsif.2020.0196 . hal-03005659

HAL Id: hal-03005659

<https://hal.science/hal-03005659>

Submitted on 14 Nov 2020

HAL is a multi-disciplinary open access archive for the deposit and dissemination of scientific research documents, whether they are published or not. The documents may come from teaching and research institutions in France or abroad, or from public or private research centers.

L'archive ouverte pluridisciplinaire **HAL**, est destinée au dépôt et à la diffusion de documents scientifiques de niveau recherche, publiés ou non, émanant des établissements d'enseignement et de recherche français ou étrangers, des laboratoires publics ou privés.

**Subject Areas:**Biomaterials, Biophysics, Systems
Biology**Keywords:**Bacterial colonies, Structural color,
Photonic crystals, Living optical
material**Author for correspondence:**

Silvia Vignolini

e-mail: sv319@cam.ac.uk

Complex photonic response reveals 3D self-organization of structural colored bacterial colonies

Lukas Schertel¹, Gea T van de Kerkhof¹,
Gianni Jacucci¹, Laura Catón¹, Yu
Ogawa², Bodo D Wilts³, Colin J Ingham⁴,
Silvia Vignolini¹ and Villads E Johansen¹¹University of Cambridge, Department of Chemistry,
Lensfield Road, Cambridge, CB2 1EW, United Kingdom²University Grenoble Alpes, CNRS, CERMAV
Grenoble, France³Adolphe Merkle Institute, University of Fribourg,
Chemin des Verdiers 4, CH-1700 Fribourg, Switzerland⁴Hoekmine BV, Room 1.091 (iLab), Kenniscentrum
Technologie en Innovatie, Hogeschool Utrecht,
Heidelberglaan 7, 3584 CS, Utrecht, The Netherlands

Vivid colors found in living organisms are often the result of scattering from hierarchical nanostructures, where the interplay between order and disorder in their packing defines visual appearance. In the case of *Flavobacterium* IR1, the complex arrangement of the cells in polycrystalline three-dimensional lattices is found to be a distinctive fingerprint of the colony organization. By combining analytical analysis of the angle-resolved scattering response of in-vivo bacterial colonies with numerical modelling, we show that we can access the inter-cells distance and cell diameter with a resolution below 10 nm, far better than what can be achieved with conventional electron microscopy, suffering from preparation artefacts. Retrieving the role of disorder at different length scales from the salient features in the scattering response enables a precise understanding of the structural organization of the bacteria.

1. Introduction

Iridescent structural colors originate from the interference of light scattered from transparent materials organised at a nanoscale level. In contrast to dye/pigmentation-based coloration originating from absorption, such structural colors allow living organisms to fully control their visual appearance both in terms of color and angular distribution. In fact, periodic arrangements of nanostructures in 1,2 or 3 dimensions can cause very bright, angle-dependent structural colors [1], as expected for photonic crystals [2–7], while matt, homogeneous color arises from short-range correlation of scatterers [8] or resonant scattering phenomena in disordered structures [9–11].

In case of periodic structures, diffraction has been used to assess bacterial dimensions as long as 100 years ago [12–14] and structural color in bacteria was noted in the literature as long ago as 1941 [15]. Recently, a number of Flavobacterial strains have been reported to grow in colonies that display structural color [16–18]. However, a detailed explanation on how the interplay between order and disorder in their packing dominates the optical appearance in this system remain unclear. Such knowledge would allow insights into the bacterial colony behavior and enables their use as living optical materials.

In this manuscript, we used the *Flavobacterium* strain IR1 (wildtype, WT) [18] as a model system to study how the 3D polycrystalline organization of rod-shaped bacteria creates structural color (see Fig. 1a and Fig. S1). Through analytical and numerical models, we assessed the lattice length of the packing with a resolution below 10 nm and estimate the value of the refractive index of their environment providing insights on the material used in their extracellular matrix. Moreover, we were able to extract information about the crystalline organization of the cells, their orientation, as well as the packing fraction by correlating all observed spectral features to physical mechanisms. Inducing deviations from the perfect crystal lattice arrangement of the bacterial positions in numerical simulations and the analytical analysis allows us to learn about the degree of disorder present on multiple length scales in the bacterial samples.

The obtained results enable further studies of the self-organizational capacity of bacterial colonies, as a thorough understanding of the structure-function relation of bacterial colonies opens new ways to the modification and use of these bacteria for a range of technological applications.

2. Results

Bacterial colonies acting as photonic systems

Flavobacterium IR1 was cultivated on Artificial Sea Water Black (ASWB, see Methods) agar in a Petri dish. As shown in Fig. 1a, a strong angle-dependent color appearance is observed. For small illumination angles with respect to surface normal ($\theta_i = 0^\circ, 10^\circ$) the colony appears blue with a very low scattering intensity, while for larger angles ($-45^\circ, -60^\circ$) we can observe a strong green scattering response (see Methods for details and Fig. 1b for a schematic of the measurement geometry). In the growing edge of the colony the color is red-shifted, however in the following we will consider only the centre of the colony as the growing edge still organizes and reorganizes as well as similar green appearances have been reported in earlier studies [16,18–20].

Structural organization of bacteria. An overview of the structural organization of IR1 bacterial colonies is obtained with a combination of Electron Microscopy (EM) techniques (Scanning EM, cryogenic-SEM and Transmission EM) as shown in Fig. 1c-f. The SEM image in Fig. 1c shows an edge of the colony allowing insights into the bacterial organization. The positions of the bacteria are strongly correlated in space (Fig. 1d) and such correlation can be observed across all the colony (see also SI in ref. [18]). A hexagonal packing is clearly recognisable in cryo-SEM cross-section imaging (Fig. 1e, see Methods for details) and TEM (Fig. 1f, see Methods for details). However, large-area imaging both via cryo-SEM images (Fig. S2a and b) and TEM (Fig. S2d) reveals that the

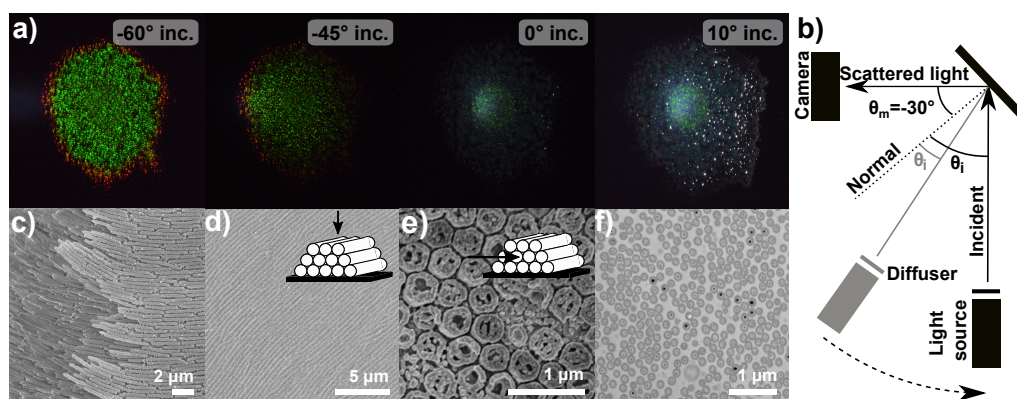


Figure 1. Bacterial film imaging and appearance: a) Images of a bacteria colony for constant angle of observation ($\theta_m = -30^\circ$) but varying angle of incidence. Left to right: $\theta_i = -60^\circ, -45^\circ, 0^\circ, 10^\circ$. b) Sketch of the scattering geometry for taking images with a camera, c) Scanning electron microscopy image (SEM), d) cryogenic SEM top-view (Inset: sketch of the geometry), e) cryogenic SEM cross-section (Inset: sketch of the geometry), f) Cross-section in transmission electron microscopy (TEM).

bacteria are aligned in a hexagonal lattice locally, but that there is no long-range correlation in their orientation. In fact, each domain shows local order on a length scale which is comparable to the coherence length of incidence light. Therefore, when measured on a larger scale ($\sim 100\mu\text{m}$ [18]) all possible in-(surface)plane rotations of the lattice can be expected. This observation is in agreement with the structural color appearance that shows no angular dependency with in-plane rotation (Fig S4 in [18]) and allows us to model the bacterial colony as domains of packed bacteria with local order and random orientation on a larger scale as visualised in Fig. S2c.

However, while the EM imaging techniques provide a very good qualitative description of the organization of the cells, the precise measurement of the value of the lattice constant d (inter bacteria distance) from these images remains challenging due to sample preparation artefacts. In fact, TEM image analysis of the structure in Fig. 1f reveals a lattice constant (inter bacteria distance) of $d = 179 \pm 17$ nm, which is less than half of what we measure from the cryo-SEM cross-section (Fig. 1e, $d = 414 \pm 29$ nm). Such values differ also from the cryo-SEM top view images where the lattice constant is $d = 374 \pm 36$ nm if measured by a lineplot (see Fig. S3) and is $d = 396 \pm 36$ when estimated by autocorrelation image analysis as described by Johansen and coworkers [18], where the authors obtained a value of 357 nm from a SEM top view image. Interestingly, while the absolute values of d differ between the different methods, the ratio between the bacterial size a and lattice distance d remains similar for all methods within errors ($\frac{a}{d} = 0.9 \pm 0.05$), revealing that the artefacts are mainly connected to shrinking caused by dehydration of the colony. Cryo-SEM imaging suffers less from dehydration artefacts but quantitative values of d are difficult to achieve deep inside the colony, as ice crystal growth becomes an increasing issue away from the sample surface [21]. The overall sample thickness is estimated from Cryo-SEM cross sections (Fig S2e) to be 10-15 μm . Moreover, as the cell orientation varies within the colony, the measured d is often not measured in a cross-section image that is perpendicular to the orientation of the cells. This can be seen in Fig. S2d, where the same sample is imaged at different locations in cross-section leading to different absolute lattice values and sizes. On the other hand, when the structure factor of fixed colonies is evaluated from TEM and SEM images (see Fig. S4), good hexagonal packing is observed. Therefore this technique provides a very good overview of the ordering of the sample especially deep inside the colony, where the cryo-EM methods fail.

Goniometry as an advanced characterization tool. In order to evaluate the value of d without perturbing the colony we recorded angle-resolved reflectance spectra with an optical goniometer

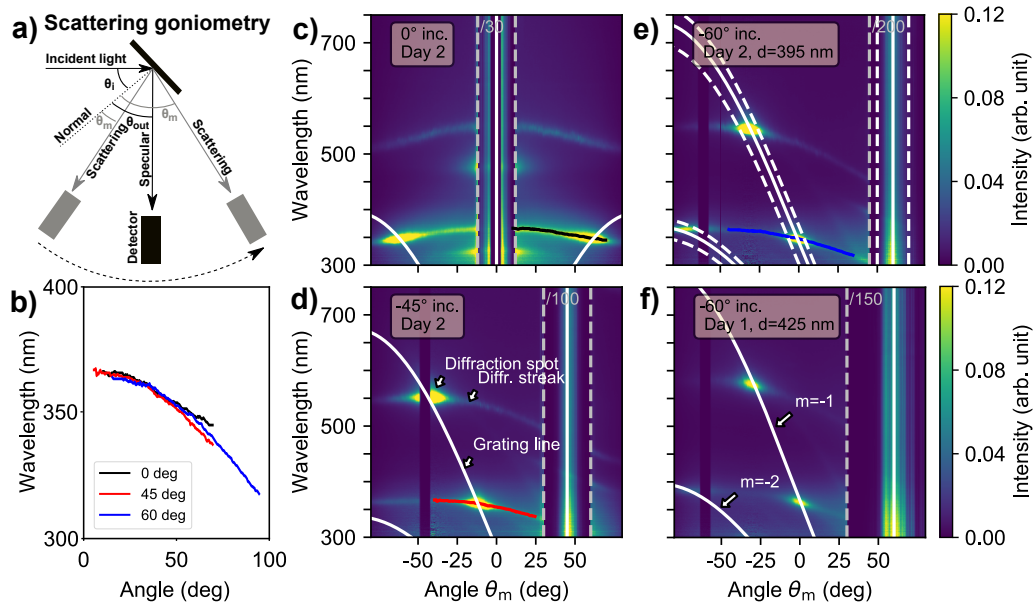


Figure 2. Diffraction of bacterial colonies at different scattering geometries: a) Sketch of the scattering goniometry setup. b) Diffraction streak lines corrected for their incident angle extracted from c)–e). Scattering goniometry measurements for c) $\theta_i = 0^\circ$, d) -45° and e) -60° incident angle for a WT IR1 sample from day 2. f) -60° incident angle measurement for a WT IR1 sample from day 1. White lines indicate the analytical solution of the grating equation (eq. 2.1) of the indicated lattice constant d . Dashed white lines in e) show the same equation indicating an uncertainty in incident angle by $\pm 10^\circ$.

setup. This technique has the advantage of probing a large area of living colonies without the need for any sample preparation. Figure 2a shows the schematics of the geometry used in our experiment for a scattering configuration where the illumination is fixed at one angle and the scattering from the sample is measured at all the other angles (see Methods for details of the setup). Similarly a specular-reflection configuration can be measured (see Fig. 3a), where the angle of illumination always equals the angle of observation. The specular reflection ($\theta_{in} = -\theta_{out}$) is measured in the range $\theta_{in} = -45^\circ$ to 45° , while the scattering properties of the sample are collected for the light incidence angles $\theta_i = 0^\circ$, -45° and -60° with respect to the sample normal. The scattering goniometry data shown in Fig. 2c–e together with the structural characterisation by electron microscopy, will be the foundation for the subsequent analysis.

Analytical analysis allows structure determination

Figure 2c–e shows three scattering goniometer measurements for the light incidence angles of $\theta_i = 0^\circ$, -45° and -60° of a sample cultured for two days in an incubator at 25°C , measured in the centre of the colony. For the investigation a piece of agar ($\sim 2 \times 2$ cm) with the colony was simply cut out from the Petri dish, attached to a glass slide using double-sided tape and then mounted on the goniometer setup. In all measurements, a region of $\sim 5^\circ$ around the angle of incidence shows no signal caused by the limitation in the design of the setup (the detector arm overlaps the source). In the following logic, we aim to uncover the structural origin of all observed features by assigning them to their physical mechanisms. Small changes in the optical appearance can be detected by goniometry [18] and if related to their structural change, this will reveal changes in the bacterial organization.

As expected from the EM image analysis, we observe a scattering response that can be attributed to a polycrystalline two dimensional structure with hexagonal packing in cross-section.

In our configuration, only the scattering from bacterial domains aligned perpendicular to the goniometer detector plane will contribute to the recorded scattered data (see sketch in Fig S2c). In fact, the measured angle-resolved reflection for any domain and any illumination is consistent with conical diffraction (see Fig. 1,2,3 in [22]). More in detail, in Fig. 2c-e we can recognise several distinct features in the optical response of the bacterial colony. In the following, we provide a phenomenological, but quantitative description of these features derived from closed-form expressions and use this to extract the relevant parameters determining the optical response of the colony.

Lattice constant retrieval from diffraction spot. Diffraction grating-like structures are formed by the bacterial colonies (see for example the cryo-SEM top view Fig. 1d). The lattice constant, corresponding to the inter-bacterial distance, can be directly obtained from the experimental goniometer data (Fig 2). The angles of constructive interference from a diffraction grating can be expressed by the grating equation

$$\theta_m = \arcsin \left(\frac{m\lambda}{d} - \sin \theta_i \right), \quad (2.1)$$

where $m \in [0, -1, +1, -2, +2, \dots]$ is the order, λ is the wavelength of light, d is the period of the structure, θ_i is the angle of incidence and θ_m is the reflection angle for a given order. By matching this equation with the high-intensity reflection spots in the scattering measurements (see white lines in Fig 2c-e) we find that the spot location indeed is governed by the grating equation. The equation estimates the periodicity to be 395 ± 5 nm. Note that this simple method allows us to achieve a very high resolution combined with a high reproducibility. An uncertainty of only ± 5 nm is obtained from fitting three different WT IR1 samples on day 2 as shown in Fig. S6. For comparison, a variation of $\Delta d = \pm 20$ nm is shown in Fig. S6a as dashed white lines. This shows a remarkable degree of reproducibility for an *in-vivo* measurement and confirms that goniometry can be far more accurate than TEM, SEM or cryo-SEM for obtaining averaged quantitative values of the packing.

The possibility to achieve such a high accuracy allows us to map efficiently different life stages of the bacteria colony. As an example, a lattice constant of $d = 395 \pm 5$ nm was obtained for day 2 (Fig 2e). The same sample is measured at day 1 (see Fig 2f) where the colony shows a slightly more red shifted diffraction spot, corresponding to a lattice constant of $d = 425 \pm 5$ nm.

Diffraction streak as indication of domain tilts in the colony. The diffraction spots in Fig. 2 show a certain width which can be related to a tilt of the sample surface by $\pm 10^\circ$ (dashed white lines in Fig. 2e). Such tilt in the orientation of the domains can in fact be observed in Fig 1a, Fig. S3e and Fig. S3f on the sample surface. Note that the bacteria still grow mainly as a flat film on the agar plates but a certain local deviation from that is expected to occur in bacterial colonies. Similarly, earlier reports show that buckling is a common phenomenon in bacterial colonies [23–25] and calculations by Kientz and co-workers [20] suggest such effect to be present in structurally colored bacterial colonies.

Remarkably we observe, in the proximity of the diffraction spot, a significant spread of intensity (diffraction streak). This spread stretches over the whole angular range and crosses the specular reflection even for normal incidence ($\theta_{in} = 0^\circ$) where the higher wavelength diffraction spot is out of the measured angular range. Such spread cannot be caused by tilts in the sample surface, variations in the lattice constant of the periodic arrangement of the bacteria or other types of disorder, such as orientational disorder within one crystalline unit cell. We expect this streak to originate from tilted domains within the colony. To confirm that tilted domains within the colony are responsible for the streak line of the diffraction peaks, we extracted the low wavelength scattering features in Fig 2c (black line), d (red line) and e (blue line) and corrected them for the angle of incidence of the light. From geometrical considerations it follows that a shift in input angle corresponds to a similar shift in output angle (Fig S5a). In Fig. 2b we observe that the extracted scattering behaviour overlays on each other once corrected for the angle of tilt, suggesting that the streaks indeed originate from tilted domains. The observation of the spread of intensity around the diffraction spots over the whole angular range allow us to conclude that a large variety of

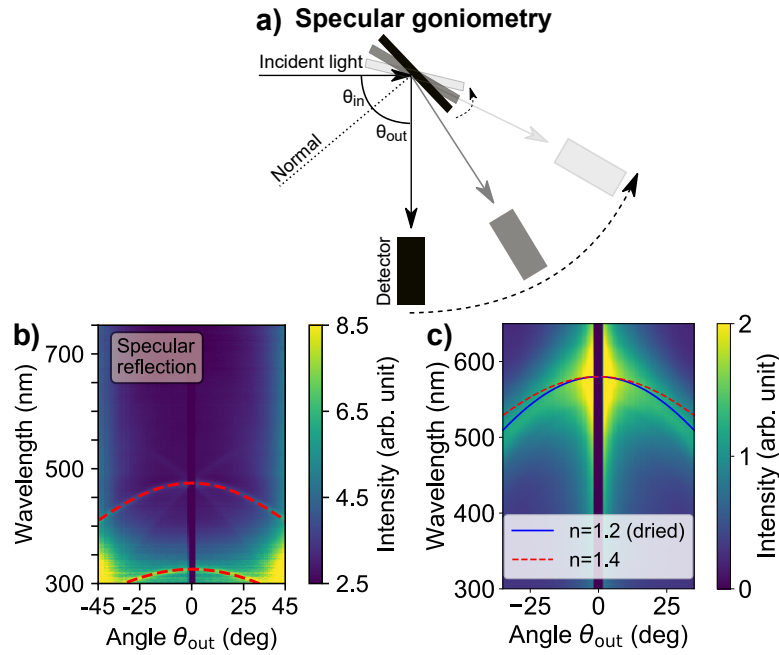


Figure 3. Specular reflection of bacterial colonies: a) Sketch of the specular goniometry setup. b) Specular measurement for a WT IR1 sample from day 2 with an overlay of the analytical solution eq. 2.2, dashed red line; c) Specular measurement and fit (blue line) of a dried and fixed WT IR1 sample. Refractive index result from b) shown as red dashed line for comparison.

tilts are present in the sample. Note that the diffraction spots still governs the signal intensity, meaning that most domains grow flat and parallel to the agar surface.

Refractive index retrieval from angle-dependent specular reflection. The optical data allows the extraction of another key parameter for photonic systems, its effective refractive index. The specular reflection peaks for a specific angle θ_{out} are caused by the constructive interference of waves travelling in the medium at an angle given by Snell's law $\theta_2 = \arcsin \frac{\sin \theta_{in}}{n_{avg}}$, where θ_{in} is the illumination angle and n_{avg} is the volume average effective refractive index of the total material composite in the photonic crystal. Inside the sample, the optical path length changes with the z -projection of the wave vector, meaning that it is the cosine-projection of the distance the wave travels that determines the constructive interference criterion (Fig. S5b). Therefore the peak reflection wavelength λ_p for normal incidence is shifted in angular space to a shifted peak wavelength λ_s as follows:

$$\lambda_s = \lambda_p \cos(\theta_2) = \lambda_p \cos\left(\arcsin \frac{\sin \theta_{in}}{n_{avg}}\right). \quad (2.2)$$

λ_p can be extracted from the specular measurement (Fig 3b) by reading out the wavelength where the specular line crosses 0° . Then equation 2.2 can be used to fit n_{avg} to the specular reflection curve profile (red dashed lines in Fig. 3b). The fitting procedure determines the average refractive index to $n_{avg} = 1.4 \pm 0.05$. This is close to the reported values of $n_{bac} = 1.38$ and $n_{agar} = 1.34$ for another *Flavobacterium* grown on an agar plate [20]. For measurements on a dried sample, we obtain $n_{avg} \approx 1.2 \pm 0.05$ (see blue line in Fig. 3c), which indeed confirms the drying out of the material compared to the live, hydrated state. We conclude that this method is a quick way to estimate or confirm the refractive index range of an unknown system, and can directly be used to

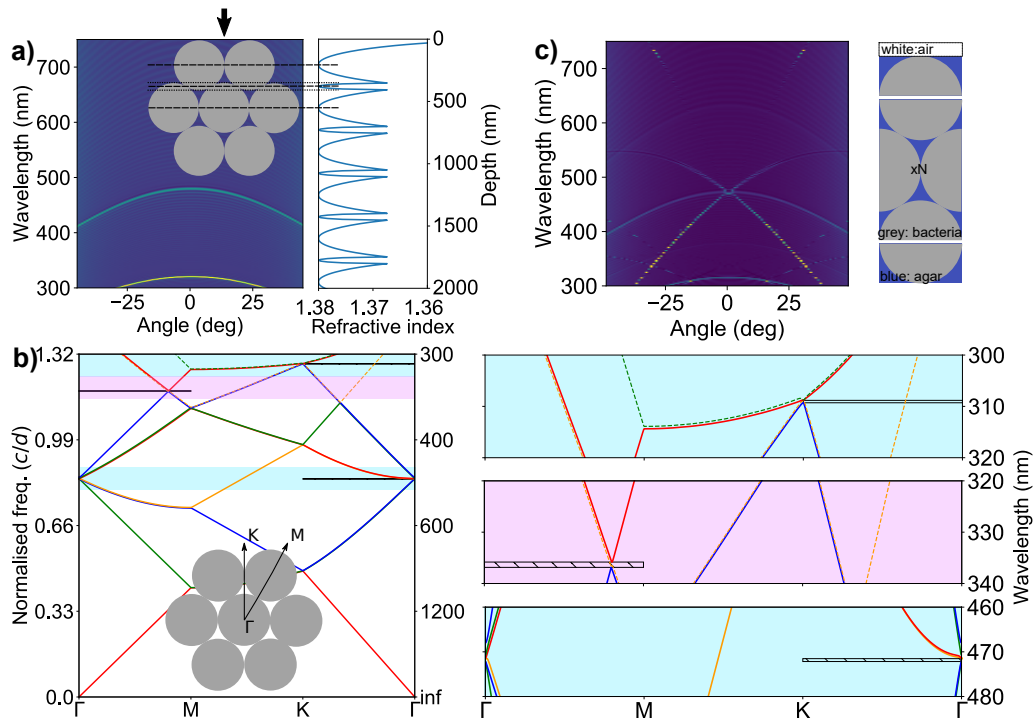


Figure 4. Optics of a low refractive index contrast 2D photonic crystal: a) Left: Multilayer 1D transfer matrix simulation with layers as indicated in the sketch (inset), black arrow indicates normal surface incidence) Right: refractive index structure used for the multilayer calculation. b) MIT Photonic Band (MPB) simulation showing the band structure of a hexagonal crystal. Inset: Sketch of the crystal with indicated direction where photonic bandgaps were found. Right: zoom ins to the photonic bandgap positions. Horizontal black(hatched) lines indicate partial band gap position. c) FEM simulation of the hexagonal lattice of finite thickness with $N=41$ repeating unit cells. The repeating structure is sketched on the right.

investigate the composition of the extracellular matrix although more precise techniques [26,27] are needed to better resolve the refractive index precisely.

Numerical analysis of a crystalline bacterial arrangement

In the following, we provide a full description of the optical response from the bacterial colony by finite element calculations. We further present a bandgap analysis of the photonic crystal structure to provide a more intuitive insight on the propagation of the electromagnetic modes inside the bacterial colony. These results uncover the physical origins of the optical response of the studied sample.

In Figure 1c, we observed that the bacterial stack in tightly packed layers, forming a hexagonal arrangement in cross-section (Fig. 1e, f). In a first approximation, the optical response can be obtained by using a 1D transfer matrix approach [28,29] (see Methods) with a refractive index structure as pictured in Figure 4a (right). In this case we assumed the refractive index of the bacteria to be $n_{\text{bac}} = 1.38$ and the surrounding matrix $n_{\text{env}} = 1.34$ in agreement with previous reports [20]. The angular dependency of the multilayer system is studied by changing the angle of incidence and measuring the wavelength-resolved reflectance. The result shown in Fig. 4b reveals that this simplified simulation of the 2D photonic crystal structure already predicts the specular reflection response measured experimentally.

Bandgap analysis confirms 2D hexagonal photonic crystal. To further understand the origin of the specular reflection and diffraction peaks, a photonic bandgap analysis on a hexagonal 2D photonic crystal structure was performed using the MIT Photonic Bands code [30] (Fig. 4b). In this calculation, the input parameters are the lattice constant ($d = 395 \text{ nm}$) and the tabulated refractive indices. The result of this analysis shows similar behaviour for both transverse electric (TE) and transverse magnetic (TM) polarisation. Therefore, in this section we will only discuss the results for the TM modes in Fig. 4b and refer to Fig. S7b for the TE modes. In Fig. 4b note that the dashed lines correspond to asymmetric modes while the solid lines correspond to symmetric modes. The symmetry of the modes was identified in Fig. S7a. Asymmetric modes can be disregarded when searching for bandgaps as they cannot be excited by an incident plane wave [31].

From the bandgap diagram, three partial band gaps in the visible light range are found manually. The two bandgaps in the ΓK -direction are at 309 nm and 471 nm (light blue background) and correspond to the direction where light is incident perpendicular to the colony surface. The gaps are both less than 1 nm (see Fig. 4b zoom on the right), owing to the low refractive index contrast, such that mode banding can not be excluded. Despite their small spectral width these two band gaps can still lead to a noticeable signal in the experiments as they form the origin of the specular reflection lines. It is worth noticing that the visible light reflections in the experiments originate from band gaps between higher bands and not the first band, which would require roughly twice the bacterial cell size. This seems to be different from other natural photonic crystal systems [32–34].

Another bandgap is found in the ΓM -direction at 336 nm (magenta background) corresponding to a 30° (or -30°) tilt of the structure. Interestingly, the appearance of one of the band gaps in the UV part of the optical spectrum may provide a functional adaptation of the bacterial colonies in providing a UV protection mechanism. To further understand the optical signal corresponding to this gap we simulated the angular resolved reflectance of a multilayer tilted by 30° and -30° approximating the hexagonal structure as sketched in Fig. S8a. Although the experimental case is different, the observed features can be related to two weak signals observed in the specular measurements seen as crossing lines of the high wavelength specular line (see arrows to rescaled specular measurement in Fig. S8). In the experiments we observe that, the signal coming from tilted layers with respect to the sample normal (see Fig. S8a) is weakened in intensity compared to the symmetric specular lines.

Finite element method reveals photonic bandgap lines. In order to confirm the parameters established from the analytical analysis and prior literature, as well as to check our predictions from the bandgap analysis and multilayer simulations, we simulated the specular and diffracted reflection using the finite element method (FEM). Combining FEM with a transfer matrix formalism, we can resolve Maxwell's equations for the full system, including the air interface and the substrate interface. In this model, we only assumed a periodic, hexagonal packed bacterial colony with a period of 395 nm as extracted from eq. 2.1, and the refractive indices of $n_{\text{bac}} = 1.38$, $n_{\text{agar}} = 1.34$. We use an in-house finite element solver [35,36] combined with a transfer matrix method [37] for efficient reflection calculations of the periodic layers of bacteria, meaning that only one layer of bacteria were simulated and the solution then repeated N times to obtain the overall scattering characteristics (Fig. 4c). This result shows excellent agreement with the specular measurements as shown with a rescaled intensity in Fig. S8c. All specular lines are recovered by the FEM modeled hexagonal packed crystal structure. Given the model assumptions, the prediction of the reflection wavelengths is fairly accurate. The reflection bandwidths are much more confined, which is to be expected for a completely periodic model system. In contrast to all earlier introduced studies, the FEM calculations allow us to study the effect of the photonic band gaps on higher order diffraction. By plotting the first order diffraction spectra for varying angles of incidence (see Fig. S8d), we find that the high wavelength diffraction giving rise to the strong green appearance of the bacterial colonies only sets in for incident angles larger than $\theta_{\text{in}} \approx 20^\circ$.

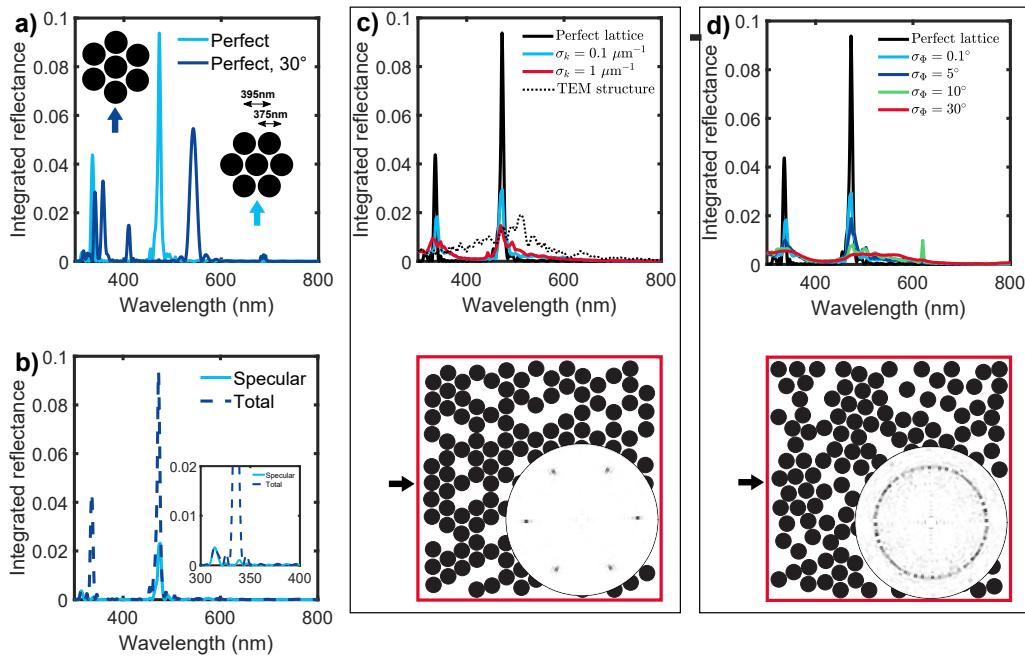


Figure 5. Introducing disorder in a photonic crystal lattice: FDTD simulations of spheres packed in a hexagonal lattice with diameter 375 nm, lattice distance $d = 395$ nm, filling fraction $f = 0.6$ and sample volume $5 \times 5 \mu\text{m}$ (constant number of spheres). a) Angular integrated reflectance for two different crystal orientations in respect to the incident light (see arrows and sketch in inset). b) Specular and total integrated reflectance of the "perfect" lattice from a). c) Integrated reflectance of the hexagonal lattice with increasing disorder in the particle distance. σ_k is the error (standard deviation) of the module of the wavevector k . Exemplary structure shown below the figure with corresponding structural correlation in angular space. For comparison the reflectance spectrum calculated with FDTD from a structure extracted from a TEM image (see Figure S4) is shown (dashed-dotted line). d) Integrated reflectance of the hexagonal lattice with increasing disorder in the particle angular orientation. σ_ϕ is the standard deviation of the angle Φ relative to the incident wave vector. Exemplary structure shown below the figure with corresponding structural correlation in angular space. Incident light direction indicated by black arrows.

Learning from disorder

In the bandgap analysis as well as the FEM study we assumed, the bacteria were forming a perfect hexagonal crystalline lattice from touching hard disks in cross-section. In contrast, in EM cross-sections (Fig. 1e, f) we observed that the bacteria resemble more soft disks with a certain degree of packing and orientational disorder. To account for such effects we therefore perform finite difference time domain (FDTD) simulations [38,39].

Perfect lattice reveals crystalline orientation. In all FDTD calculations we study the integrated total reflection for normal incidence of a plane wave. As shown in Fig. 4, the direction of normal incidence on the hexagonal structure corresponds to the $K\Gamma$ direction. We first investigate the effect of the orientation of the hexagonal packing in respect to the incident light. The total reflectance of the perfect hexagonal lattice with lattice constant of $d = 395$ nm is simulated for two crystal orientations in Fig. 5a.

For incidence in $K\Gamma$ direction, two strong peaks at 336 nm, 473 nm and one weak peak at 313 nm are obtained in correspondance with experimentally observed features while the $M\Gamma$ incidence leads to a spectrum with five peaks in the visible range, in contradiction with the situation observed in the experiments.

In Figure 5b, we compare the total integrated reflectance with incidence in $K\Gamma$ direction with the spectrum of the specular reflection and find that the peaks at 313 nm and 473 nm correspond to the specular reflection while the peak at 336 nm correspond to the first order diffraction in excellent agreement with the observation in the 0° incidence measurement in Fig. 2. Note that in the experimental spectra (Fig. 2 and 3), the specular reflection peaks show higher intensities than the diffraction peak. This is not recovered in the numerical calculations as the boundary of the sample has not been taken into account and the intensities strongly depend on the domain thickness inside the colony assumed in the numerical calculations. Taking into account the sample boundary conditions, the domain thickness inside the bacterial colonies and the absorbing substrate in transmission is a challenging task, both to investigate experimentally and to calculate numerically but would allow a quantitative comparison of intensities and give further insights into the bacterial assembly.

To conclude we related the features observed in the spectra to a specific orientation of the crystalline structure as pictured in Fig. 5a (right inset). The orientation found here is expected as it allows a better packing in a two-dimensional geometry, forming a flat surface, consistent with surface energy minimization arguments.

Disorder analysis. To study the effect of disorder on the total integrated reflectance, we introduce lattice disorder (Fig. 5c) and crystalline orientation disorder (Fig. 5d) separately (see Methods for details.) The average value of the lattice constant is assumed to be the one retrieved from the analytical analysis. We expect the rod-shaped bacteria to have a diameter smaller than this value to allow for small amounts of disorder. This claim is further strengthened by the cryo-SEM cross-section shown in Fig. 1e and Fig. 1f. In these images we extracted averaged sizes at least 5% smaller than the distance. Therefore, in all FDTD simulations we used a particle diameter of 375 nm while the particle distance (lattice constant) is kept at 395 nm.

In Fig. 5c we observe that small amounts of disorder in the lattice distance (hardly visible in the simulated structure) already lead to a strong decrease of the peak intensity and a broadening of the peak width, similar reported in literature for another 2D photonic crystal [40]. A similar effect is also observed for the disorder in angular alignment within the hexagonal crystal as introduced in Fig. 5d. Here, already small amounts of disorder can be observed in the real structure (Fig. S9). Complete angular disorder (see red line and corresponding structure as well as isotropic angular space distribution in Fig. 5d) leads to a broad spectrum with no distinct peaks in the visible range. Despite the low refractive index contrast in our samples, a remarkably bright angle-dependent color appearance is observed in the measurement. From this, we conclude that a high degree of order within each crystalline domain remains in the studied samples.

The FDTD method can further be applied to real structures imaged by TEM or Cryo-SEM in cross-section. A TEM image is converted in a binary image (Fig S4) and the total angular integrated reflectance spectrum is calculated. The result is shown in Figure 5 as black dotted line. A very broad peak around 510 nm is observed strongly deviating from the experimental results. This emphasizes that goniometry in comparison with numerical tools allows more insights into the structural arrangement of living microorganisms than EM imaging methods only.

3. Conclusion

In summary, we studied the interplay between order and disorder in the structural organization of iridescent bacterial colonies. By correlating angle-resolved measurements with simple closed-form expressions, we were able to deduce the inter-cellular spacing as well as estimate the average refractive index of cells and their matrix.

The combination of analytical scattering analysis, multilayer simulations, bandgap analysis and finite element calculations allowed us to recover the origin of all optical features observed in specular and scattering goniometry measurements. Moreover, the quantitative characterization of the broadening of the diffraction peak led us learn about the degree of disorder on domain alignment and enables further studies of bacteria communication under different growth

conditions: as an example it might be useful in estimating the physical interactions of cells during adaptation of the colony structure in response to environmental conditions.

In conclusion, our in-vivo, non-invasive method is particularly important for biofilm characterization as bacterial colonies and biofilms are known to be differentiated dynamic structures [41,42] and traditional methods rely often only on imaging studies confined to monolayer microcolonies [43] or static sectioning approaches. Additionally, our finding can be extended to any other two-dimensional photonic tissue in other organisms as the response only depends on the size ratio between the scattering elements and the optical wavelength.

4. Materials and Methods

Sample isolation

Strain IR1 was isolated on ASW agar during a screening of estuarine sediment samples from the Neckarhaven region of Rotterdam harbour [18]. Strain IR1 is a yellow-pigmented Gram-negative bacterium culturable on ASW agar under aerobic conditions from 2 to 30°C with salinity matching the location where it was isolated (0.5–1.5). On ASWB plates, containing nigrosine as a contrasting agent, IR1 formed intensely structurally colored green colonies with red/orange edges as seen in Fig. S1.

Sample preparation

Bacteria were grown on ASWB agar plates, containing 17.5 g agar (Invitrogen), 10 g KCl, 1 g yeast extract (Sigma: Y1625), 5 g peptone (Sigma: 70173) and 0.33 g nigrosin (Sigma: N4763) per litre. Plates were allowed to dry to air for 30 minutes after which bacteria were added, and then dried to air for another 15 minutes. Bacteria were inoculated on the plates by suspending them in a 1% w/v KCl solution, of which 5 μ L was deposited on the plates. These plates were placed into an incubator at 25°C for one/two days before measuring.

Photographic images

A directed beam from a xenon lamp (HPX2000, Ocean Optics) was used as a light source. A white sheet was put in between the beam and the sample to simulate a diffusive, but directed illumination. All images were taken with a camera (Nikon D3200).

Scanning Electron Microscopy

The SEM studies (Fig. 1c) were performed on fixed colonies that resulted in the dried material maintaining a structural color described elsewhere (see SI in Johansen *et al.* [18]).

Cryogenic SEM

Cryo-SEM was performed on a FEI Verios 460 scanning electron microscope with a Quorum cryo-transfer system PP3010T. A piece of agar (2x2 cm) with bacteria was cut out and placed in a specimen holder with colloidal graphite suspension. The specimen holder plus sample was then plunge frozen in liquid ethane and transferred to a specimen preparation chamber cooled down to approximately -140°C. Samples for cross-sectional view were then freeze-fractured, all samples were sublimed at -90°C and sputter-coated with platinum. All samples were imaged at 2.00 kV acceleration voltage.

Transmission Electron Microscopy

Samples were embedded for TEM by chemical fixation. Small pieces of the bacteria colony on agar gel were cut out and fixed with glutaraldehyde (2 wt%) and formaldehyde (2 wt%) in 0.1

M sodium cacodylate buffer (pH 7.5) overnight at 4°C. During the fixation the bacteria colony had detached from the agar which was subsequently removed. Samples were then rinsed with the buffer solution and post-fixed in an OsO₄ solution buffered at pH 7.4 for 2 hours at 4°C. The samples were then washed with deionized water and dehydrated through a graded ethanol series (30 to 100%) to dry acetonitrile. They were left in a mixture of 50% dry acetonitrile and 50% Quetol 651 epoxy resin overnight, followed by infiltration in Quetol resin for two days. Samples were placed in a silicon mold with Quetol resin and cured for two days at 65°C. Ultrathin sections were cut using an ultramicrotome Leica Ultracut E. with a 45° diamond knife (Diatome). Sections were placed on carbon-coated copper grids and post-stained with 2 wt% uranyl acetate aqueous solution and Reynolds lead citrate solution. They were imaged in a FEI Tecnai G2 transmission electron microscope operated at 200 kV and equipped with an AMD CCD camera.

Goniometry

As light source we used a xenon lamp (HPX2000, Ocean Optics) coupled through a fibre to a reflective collimator (RC08SMA-F01) in order to produce a collimated beam with a spot size of 5 mm. The same type of reflective collimator and fiber was used to couple the light to a spectrometer (AvaSpec-HS2048, Avantes) for detection. For normalisation a white diffuser was measured at 0° incidence with the detector at 5°. For further details see [44].

Generation of 2D structures for Finite Difference Time Domain simulations

Structures with different degrees of disorder were generated following an inverse-design approach [39]: first, the desired number of hard particles were added to the system, then their positions were gradually changed in order to minimize the difference between the targeted structure factor and the one of the ensemble of particles.

FDTD simulations

The simulations were performed using LUMERICAL 8.18 (Lumerical Solutions Inc., Vancouver, BC, Canada), a commercial software based on the finite difference time domain method.

We used a fixed number of scatterers for a simulation volume of 5x5 μm with a filling fraction (ff) of $ff = 0.6$. The value of ff was decided to guarantee the same number of particles both in the disordered and in the perfect hexagonal packing. Periodic boundaries conditions in the lateral direction, i.e. perpendicular to the incoming beam, Y and perfect matching layer (PML) boundaries in the X direction were used in all the calculations.

A plane incident wave is sent into the sample and the angular integrated reflection (-90° to 90°) is measured. This corresponds to an angular integration of the 0° incidence measurement in scattering goniometry (see Fig. 2c). For each disorder configuration we averaged over seven independently generated samples. In these calculations, the effect of the air-sample interface was not taken into account.

Finite Element Method

An in-house periodic 2D finite element solver based on [37] and implemented following the recipe in [45] was used. It has been thoroughly tested in several publications [35,36]. In the following, a short explanation of some important aspects for these particular simulations are given, but the reader is referred to [37,45] for full details.

Due to the periodic boundary conditions, the electric and magnetic field at the boundaries can be resolved by infinite sums (as opposed to integrals for the general case) of exponential basis functions multiplied by a set of coefficients. These are referred to as reflection and transmission modes at the boundaries. In the FEM implementation, this sum of modes is truncated to a reasonable number, since the lowest orders are propagation modes and higher orders are

evanescent modes, whose coefficients normally tend to zero. Due to our implementation, this means that the non-periodic interfaces of the simulation model have to be of a homogeneous material in order to be described by the basis given in [37,45].

The highest computational cost in solving the FEM system is to decompose the so-called stiffness matrix in the linear FE system. It is therefore extremely fast to re-use this decomposition in order to solve for other combinations of transmission and reflection coefficients. By doing this, we can obtain a complete (up to the order truncation) description of transmission and reflection for any possible combination of incident waves (on both sides) [37]. This is represented in a transfer matrix, and such matrices can be combined to represent combined geometries. As a side note: one has to remember to calculate incident angles based on Snell's law when doing this (not mentioned in [37]). Therefore, by dividing the bacteria model as seen in the sketch in Fig. 4c, we have an extremely fast way of calculating light interaction through just one period of bacteria, and then extending the results to $2N$ number of repeated bacterial cells in the depth direction. Compared to the bandgap analysis, we therefore include the effects at the interfaces (in particular the top interface, where the plane wave couples to the bacterial photonic crystal) and the effect of a finite height of the bacterial colony. Furthermore, the approach reduces computational time dramatically (compared to a full model) and makes it feasible to use a very fine resolution ($\Delta\lambda = 2$ nm) – and also to include different incident angles. All FEM simulations for this paper were performed on a laptop computer from 2015 with two physical Intel i7 3.1GHz cores, taking less than 24 h.

The approach has a few limitations. Firstly, the scattering matrices may become imprecise or unstable due to large differences in numerical values and since matrix inversions are needed [37]. Secondly, the interfaces have to be homogeneous (so we cannot make the bacterium smaller than the period). In practice, this means that some numeric values may be slightly off compared to full models, but we found the differences to be insignificant. The scattering matrix approach was verified by simulating the reflecting of N repetitions for one wavelength using a full model for low numbers of N , and then compared to the transfer matrix result. A deviation of $< 1\%$ was generally observed.

Photonic Bandgap Calculations

Bandgap solving was performed using the open source software MIT Photonic Bands (MPB) [30]. A 2D model was run for both TE and TM modes. The ctm file and post-processing scripts for reproducing the results can be found in the data repository accompanying the paper. Since a plane wave can only couple to symmetric modes [31], we needed to detect symmetric and anti-symmetric modes. This was done manually by plotting the field of the modes and search for symmetries (Fig. S8).

1D Transfer Matrix Method

The multilayer simulations were performed by using a 1D transfer matrix method python package [46]. It simulates light propagation in planar multilayer thin films, including the effects of multiple internal reflections and interference.

Acknowledgements

This study was financially supported by BBSRC David Phillips fellowship (BB/K014617/1), the European Research Council (ERC-2014-STG H2020 639088), the European Commission (Marie Curie Fellowship LODIS, 701455), EU's Horizon 2020 research and innovation programme under the Marie Skłodowska-Curie grant agreement No. 722842 (ITN Plant-inspired Materials and Surfaces–PlaMatSu) and the Swiss National Science Foundation under project P2ZHP2_183998 and Ambizione programme grant 168223.

Data availability

All data needed to evaluate the conclusions in the paper are present in the paper and/or the Supplementary Materials and/or available at the University of Cambridge data repository (<https://doi.org/10.17863/CAM.46768>).

Conflict of interest

The authors declare that they have no competing financial interests. Hoekmine BV is involved in the commercial development of bacterial photonic materials but does not gain financially from this work.

Author contributions statement

LS, VEJ, SV, CJI, GTvK, LC planned study. LS, VEJ performed data analysis. LC and GTvK cultivated bacteria. GTvK performed goniometry and took cryo-SEM. LS took angularly resolved photographs. GTvK and YO took TEM. VEJ, CJI performed SEM. GJ and BDW performed FDTD. LS, VEJ wrote manuscript. BDW helped with manuscript. All of the authors have discussed results and commented on the manuscript.

References

1. Shuichi Kinoshita.
Structural Colors in the Realm of Nature.
World Scientific Publishing Company, 2008.
2. Eli Yablonovitch.
Inhibited spontaneous emission in solid-state physics and electronics.
Phys. Rev. Lett., 58:2059–2062, May 1987.
3. E. Yablonovitch and T. J. Gmitter.
Photonic band structure: The face-centered-cubic case.
Phys. Rev. Lett., 63:1950–1953, Oct 1989.
4. S Kinoshita, Yoshioka, and J Miyazaki.
Physics of structural colors.
Reports on Progress in Physics, 71(076401):30, 2008.
5. Shuichi Kinoshita.
Bionanophotonics: An Introductory Textbook.
Pan Stanford Publishing, 1st edition, 2013.
6. Olimpia D. Onelli, Thomas van de Kamp, Jeremy N. Skepper, Janet Powell, Tomy dos Santos Rolo, Tilo Baumbach, and Silvia Vignolini.
Development of structural colour in leaf beetles.
Scientific Reports, 7(1):1373, 2017.
7. Ainsley E Seago, Parrish Brady, Jean-Pol Vigneron, and Tom D Schultz.
Gold bugs and beyond: a review of iridescence and structural colour mechanisms in beetles (coleoptera).
Journal of The Royal Society Interface, 6(suppl_2):S165–S184, 2009.
8. Jason D. Forster, Heeso Noh, Seng Fatt Liew, Vinodkumar Saranathan, Carl F. Schreck, Lin Yang, Jin-Gyu Park, Richard O. Prum, Simon G. J. Mochrie, Corey S. O'Hern, Hui Cao, and Eric R. Dufresne.
Biomimetic isotropic nanostructures for structural coloration.
Advanced Materials, 22(26-27):2939–2944, 2010.
9. Heeso Noh, Seng Fatt Liew, Vinodkumar Saranathan, Simon G J Mochrie, Richard O Prum, Eric R Dufresne, and Hui Cao.
How noniridescent colors are generated by quasi-ordered structures of bird feathers.
Advanced Materials, 22:2871–80, 2010.
10. Villads Egede Johansen, Olimpia Domitilla Onelli, Lisa Maria Steiner, and Silvia Vignolini.
Photonics in Nature: From Order to Disorder.
Springer International Publishing, Cham, 2017.
11. Lukas Schertel, Lukas Siedentop, Janne-Mieke Meijer, Peter Keim, Christof M. Aegerter, Geoffroy J. Aubry, and Georg Maret.
The structural colors of photonic glasses.
Advanced Optical Materials, 7(15):1900442, 2019.
12. A. Pijper.
The diffraction micrometer.
South African Medical Journal, 17(18):276–282, 1943.
13. A Pijper.
Diffraction in biological structures. i. the structure of colonies of the coli-typhoid group.
South African Medical Record, 17:243–248, 1923.
14. Eric Ponder.
Diffraction patterns produced by bacteria.
Journal of Experimental Biology, 11:54–7, 1934.
15. R. Y. Stanier.
Studies on marine agar-digesting bacteria.
Journal of bacteriology, 42(4):527–559, Oct 1941.
16. Betty Kientz, Peter Vukusic, Luke Stephen, and Eric Rosenfeld.
Iridescence of a marine bacterium and classification of prokaryotic structural colors.
Applied and Environmental Microbiology, 78(2092-99), 2012.
17. Betty Kientz, Adrien Ducret, Stephen Luke, Peter Vukusic, Tâm Mignot, and Eric Rosenfeld.
Glitter-like iridescence within the bacteroidetes especially cellulophaga spp.: Optical properties and correlation with gliding motility.

- PLOS ONE*, 7(12):1–12, 12 2012.
18. Villads Egede Johansen, Laura Catón, Raditijo Hamidjaja, Els Oosterink, Bodo D. Wilts, Torben Sølbeck Rasmussen, Michael Mario Sherlock, Colin J. Ingham, and Silvia Vignolini. Genetic manipulation of structural color in bacterial colonies. *Proceedings of the National Academy of Sciences*, 115(11):2652–2657, 2018.
 19. Betty Kientz, Hélène Agogué, Céline Lavergne, Pauline Marié, and Eric Rosenfeld. Isolation and distribution of iridescent *Cellulophaga* and other iridescent marine bacteria from the charente-maritime coast, french atlantic. *Systematic and Applied Microbiology*, 36:244–51, 2013.
 20. Betty Kientz, Stephen Luke, Peter Vukusic, Renaud Péteri, Cyrille Beaudry, Tristan Renault, David Simon, Trâm Mignot, and Eric Rosenfeld. A unique self-organization of bacterial sub-communities creates iridescence in cellulophaga lytica colony biofilms. *Scientific Reports*, 6(19906):11, 2016.
 21. K. P. Ryan, W. B. Bald, K. Neumann, P. Simonsberger, D. H. Purse, and D. N. Nicholson. Cooling rate and ice-crystal measurement in biological specimens plunged into liquid ethane, propane, and freon 22. *Journal of Microscopy*, 158(3):365–378, 1990.
 22. James E Harvey and Andrey Krywonos. Radiance: The natural quantity for describing diffraction and propagation. In Katherine Creath, editor, *The Nature of Light: Light in Nature*, Proceedings of SPIE, pages 628503–12, 2006.
 23. Denis Boyer, William Mather, Octavio Mondragón-Palomino, Sirio Orozco-Fuentes, Tal Danino, Jeff Hasty, and Lev S Tsimring. Buckling instability in ordered bacterial colonies. *Physical Biology*, 8(2):026008, mar 2011.
 24. William P. J. Smith, Yohan Davit, James M. Osborne, Wook Kim, Kevin R. Foster, and Joe M. Pitt-Francis. Cell morphology drives spatial patterning in microbial communities. *Proceedings of the National Academy of Sciences*, 114(3):E280–E286, 2017.
 25. Tiejian Si, Zidong Ma, and Jay X. Tang. Capillary flow and mechanical buckling in a growing annular bacterial colony. *Soft Matter*, 14:301–311, 2018.
 26. J. Politch and M. Segal. Holographic measurements of refractive-index changes. *Opt. Lett.*, 3(1):33–35, Jul 1978.
 27. Doekele G. Stavenga, Hein L. Leertouwer, and Bodo D. Wilts. Quantifying the refractive index dispersion of a pigmented biological tissue using jamin-lebedeff interference microscopy. *Light: Science & Applications*, 2(9):e100–e100, 2013.
 28. B. Harbecke. Coherent and incoherent reflection and transmission of multilayer structures. *Applied Physics B: Lasers and Optics*, 39:165–170, March 1986.
 29. Steven J. Byrnes. Multilayer optical calculations. *arXiv e-prints*, page arXiv:1603.02720, Mar 2016.
 30. Steven G Johnson and J D Joannopoulos. Block-iterative frequency-domain methods for maxwell’s equations in a planewave basis. *Optics Express*, 8(3):173–190, 2001.
 31. Kazuaki Sakoda. *Optical Properties of Photonic Crystals*. Springer series in optical sciences. Springer, 2001.
 32. Jian Zi, Xindi Yu, Yizhou Li, Xinhua Hu, Chun Xu, Xingjun Wang, Xiaohan Liu, and Rongtang Fu. Coloration strategies in peacock feathers. *Proceedings of the National Academy of Sciences*, 100(22):12576–78, 2003.
 33. Jérémie Teyssier, Suzanne V Saenko, Dirk van der Marel, and Michel C Milinkovitch. Photonic crystals cause active colour change in chameleons.

- Nature Communications*, 6:6368, 2015.
34. Vinodkumar Saranathan, Chinedum O Osuji, Simon G J Mochrie, Heeso Noh, Suresh Narayanan, Alec Sandy, Eric R. Dufresne, and Richard O Prum.
Structure, function, and self-assembly of single network gyroid ($I4_132$) photonic crystals in butterfly wing scales.
Proceedings of the National Academy of Sciences of the United States of America, 107(26):11676–81, 2010.
 35. Bokwang Song, Villads Egede Johansen, Ole Sigmund, and Jung H Shin.
Reproducing the hierarchy of disorder for *Morpho*-inspired, broad-angle color reflection.
Scientific Reports, 7(46023):8, 2017.
 36. Jacob Andkjær, Villads Egede Johansen, Kasper Storgaard Friis, and Ole Sigmund.
Inverse design of nanostructured surfaces for color effects.
Journal of the Optical Society of America B, 31(1):164–74, January 2014.
 37. Kokou Dossou, Michael A Byrne, and Lindsay C Botten.
Finite element computation of grating scattering matrices and application to photonic crystal band calculations.
Journal of Computational Physics, 219:120–43, 2006.
 38. Lumerical Inc.
FDTD: 3d electromagnetic simulator.
 39. Gianni Jacucci, Jacopo Bertolotti, and Silvia Vignolini.
Role of anisotropy and refractive index in scattering and whiteness optimization.
Advanced Optical Materials, 0(0):1900980, 2019.
 40. Doekele G. Stavenga, Casper J. van der Kooi, and Bodo D. Wilts.
Structural coloured feathers of mallards act by simple multilayer photonics.
Journal of The Royal Society Interface, 14(133):20170407, 2017.
 41. Wook Kim, Stuart B. Levy, and Kevin R. Foster.
Rapid radiation in bacteria leads to a division of labour.
Nature Communications, 7(1):10508, 2016.
 42. James A. Shapiro.
Thinking about bacterial populations as multicellular organisms.
Annual Review of Microbiology, 52(1):81–104, 1998.
PMID: 9891794.
 43. Marie-Cécilia Duvernoy, Thierry Mora, Maxime Ardré, Vincent Croquette, David Bensimon, Catherine Quilliet, Jean-Marc Ghigo, Martial Balland, Christophe Beloin, Sigolène Lecuyer, and Nicolas Desprat.
Asymmetric adhesion of rod-shaped bacteria controls microcolony morphogenesis.
Nature Communications, 9(1):1120, 2018.
 44. Silvia Vignolini, Edwige Moyroud, Beverley J. Glover, and Ullrich Steiner.
Analysing photonic structures in plants.
Journal of The Royal Society Interface, 10(87):20130394, 2013.
 45. Kazuko Fuchi, Alejandro R Diaz, Edward Rothwell, Raoul Ouedraogo, and Andrew Temme.
Topology optimization of periodic layouts of dielectric materials.
Structural and Multidisciplinary Optimization, 42:483–93, 2010.
 46. Steven J. Byrnes.
transfer-matrix method for optics of thin and thick multilayer films.
<https://github.com/sbyrnes321/tmm>, 2018.